Environmental Earth Sciences (2019) 78:513
https://doi.org/10.1007/s12665-019-8532-5

ORIGINAL ARTICLE

A multi-parameter study of groundwater–seawater interactions along Partido de La Costa, Buenos Aires Province, Argentina

Silvina Carretero[1] · John Rapaglia[2] · Santiago Perdomo[3] · Carlos Albino Martínez[3] · Leandro Rodrigues Capítulo[1] · Lucía Gómez[1] · Eduardo Kruse[1]

Received: 28 March 2019 / Accepted: 3 August 2019 / Published online: 9 August 2019

Abstract

Submarine groundwater discharge (SGD) is a complex hydrological process which occurs at the continent–ocean interface and plays an important role in coastal dynamics. The main objective of this study was to detect groundwater discharge from the sandy freshwater aquifer towards the Atlantic Ocean along the western coast of Buenos Aires Province (Argentina) using multiple methods. ^{222}Rn as a tracer, electrical resistivity tomography (ERT), and hydrogeological information were applied to detect and quantify SGD. ^{222}Rn activity was measured in wells, at the beach (tidal pools and surf zone) and along a transect ~ 200 m from the coastline coincident with geoelectrical measurements. Groundwater depth was measured in wells, and from these data, groundwater contour maps were made. ^{222}Rn activity in wells varies from 16 and 173 dpm/L; at the beach, the values are between 28 and 48 dpm/L; and along the coastline, they oscillate between 1.3 and 20.5 dpm/L. The ERT shows a high resistivity layer close to 3–4 m depth from the sea floor indicating the presence of freshwater. Groundwater contour maps show discharge toward the continental plain to the west and toward the sea to the east. There is no precedent related to the application of these methodologies in the study area which results of interest for the knowledge of the coastal hydrodynamics.

Keywords Submarine groundwater discharge · Radon · Electrical resistivity tomography · Coastal aquifer · Argentina

✉ Silvina Carretero
scarretero@fcnym.unlp.edu.ar

John Rapaglia
rapagliaj@sacredheart.edu

Santiago Perdomo
sperdomo@carina.fcaglp.unlp.edu.ar

Carlos Albino Martínez
albinocarlos7@gmail.com

Leandro Rodrigues Capítulo
leandrorodriguescapitulo@gmail.com

Lucía Gómez
lucia_gomez@fcnym.unlp.edu.ar

Eduardo Kruse
kruse@fcnym.unlp.edu.ar

[1] CONICET, CEIDE, Facultad de Ciencias Naturales y Museo, Universidad Nacional de La Plata (UNLP), 64 nº 3, 1900, La Plata, Argentina

[2] Sacred Hear University in Dingle, Dingle Oceanworld Aquarium, The Wood, Farrannakilla, Dingle, Co. Kerry, Ireland

[3] Facultad de Ciencias Astronómicas y Geofísicas, Paseo del Bosque s/n, La Plata, Argentina

Introduction

The interaction between groundwater and seawater along a coastal zone is a complicated process, which remains only partially understood. Along many coastal aquifers, submarine groundwater discharge, defined as any movement of groundwater up across the sediment–sea interface, is a natural process where fresh terrestrial groundwater and recirculated seawater moves towards the sea. Recently, however, sea-level rise and excess pumping of groundwater for human consumption or commercial use has led to, in some cases, a decline in the hydraulic head below the sea surface, leading to salt water intrusion into fresh aquifers (e.g., Sherif and Singh 1999; Werner and Simmons 2009). In extreme cases, this intrusion may contaminate the aquifers to a point where they are no longer viable for human purposes. Particularly in coastal areas where fresh groundwater is necessary for human consumption, the processes controlling the interaction between fresh groundwater and seawater are extremely important to the future viability of a coastal community (Barlow and Reichard 2010). Many communities on barrier

islands and coral atolls are dependent on the fresh aquifer for water supply, as these islands rarely have any sufficient surficial streams/water bodies for the collection of freshwater. This is the case in Partido de La Costa, Buenos Aires Province, Argentina, where residents are completely dependent on the coastal aquifer for their freshwater resource.

Meanwhile, the discharge of groundwater to the sea, henceforth known as SGD, is, in many cases, an important process affecting the ecology of coastal areas, particularly in regions where little surface input of freshwater exists (e.g., Johannes 1980). Groundwater is often elevated in the concentration of macronutrients and other chemical constituents, and hence, the discharge of this water may represent an important part of the overall flux of nutrients to the sea (e.g., Paytan et al. 2006; Slomp and Van Cappellen 2004; Windom et al. 2006). This process is even more pronounced in areas where sewage treatment is non-existent or through septic systems, or in areas where fertilizers are used in agricultural or domestic practices. Many barrier islands are composed of highly permeable sand, and therefore, any nutrient enrichment at the surface will likely lead to nutrient enrichment in the aquifer. Therefore, any movement of water from the land to the sea may increase nutrient loading in the coastal zone exacerbating associated processes. It is, important, therefore to increase our understanding of groundwater–seawater interaction in coastal zones; indeed, this process takes on increasing importance in the face of sea-level rise and global climate change (Carretero et al. 2013a).

To better understand this process, integrated techniques for assessing groundwater–seawater (GW–SW) interaction should be considered. Coastal groundwater studies are often investigated from the land side (aquifer parameters—i.e., hydraulic gradients and Darcy's Flow) or from the sea side (SGD measurements via seepage meters or chemical tracers), but rarely both (Mulligan and Charette 2006). A disconnect, therefore, exists between investigations concerned with coastal ecology and investigations concerned with the fresh groundwater resource. Multiple techniques concerning aquifer properties (well measurements), SGD tracing (radon activity), and geophysical measurements (electrical resistivity) can, therefore, be used to bridge the divide between hydrogeology and marine chemistry.

Classical hydrogeology is based on an understanding of aquifer parameters via well measurements. Along a barrier island, the freshwater lens will discharge to the sea depending upon the hydraulic head and the permeability of the aquifer via Darcy's Law. Total flow can be calculated based on these values and an understanding of discharge or saltwater intrusion can be quantified. Radon is a naturally occurring daughter of uranium. Being a noble gas, it is dissolved in water as water passes through rocks and remains in solution until exposed to the open air. Radon, therefore, is an excellent tracer of groundwater flow. Radon activity has been successfully used to quantify SGD in many coastal locations (e.g., Cable et al. 1996; Burnett and Dulaiova 2003; Rapaglia et al. 2015), and the use of Rn as a tracer is gaining increasing popularity due to the ease of measurement from the widely available Rad-7 radon-in-air detector. Geophysical measurements, while not yet as popular in the field of GW–SW interactions, provide a powerful tool in the search for subsediment anomalies (Stieglitz et al. 2008). Electrical resistivity can be used to delineate the location of fresh porewater vs. salty porewater. This information can provide an idea of the direction of flow of water in sediments. Fresh porewaters suggest flow is exiting the sediment, while salty porewater suggests the opposite.

Herein, we look at GW–SW interaction along the Partido de La Costa (PDLC) region in Buenos Aires Province, Argentina via the techniques described above. PDLC is a partially developed barrier system along the Atlantic coast of Argentina. Seventy thousand (70,000) year round residents are augmented by a vast amount of summer tourists exhibiting great pressure on the local groundwater resources. Several areas along the barrier system are already affected by saltwater intrusion, while areas with better water management techniques maintain high water quality. Our multiparameter study of the groundwater system was performed to shed some light on the current state of the GW–SW system as well as point to potential areas of concern as sea-level rises and climate changes.

Site description

Partido de La Costa (La Costa District; 36°44′S; 56°41′O)—the sandy coastline of Buenos Aires Province—is one of the most important tourist destinations in the country. It is a sand-dune barrier system increasing in height from north to south and has about 70,000 permanent inhabitants (Fig. 1). The population increases considerably during the summer due to tourism which is the main economic activity of the area. The entire population depends on the shallow aquifer for their potable water supply (Carretero and Kruse 2010). As most of the localities do not have a public drinking water supply, much of the population receives its freshwater by means of individual domestic wells, without water treatment.

The sand-dune barrier extends along a length of 70 km between Punta Rasa, to the north, and Punta Médanos, to the south, with a width ranging from 2 to 4 km. To the west, it is bordered by the vast, flat continental plain whose maximum height is 2 m.a.s.l. and is characterized by the predominance of silty and clayey sediment, separated by gullies oriented in a southeast–northwest direction which drain towards the Samborombón Bay. The dunes in the barrier are low, with heights

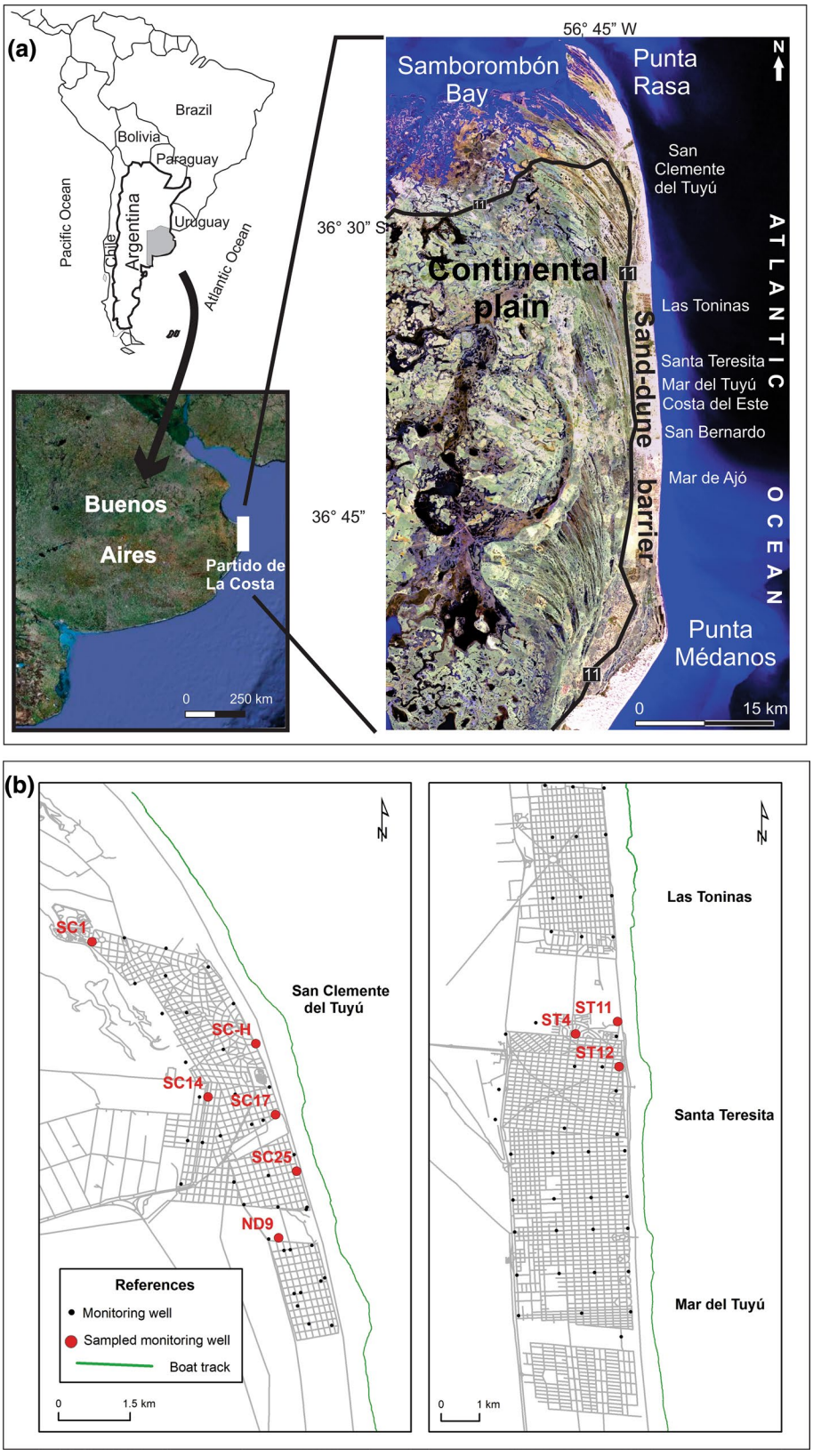

Fig. 1 **a** Study area and **b** sampling area

between 2 and 11 m.a.s.l. and fixed by sparse vegetation. The soil is sandy and is excessively drained and unstable.

The main freshwater aquifer is composed of dune sands (aeolian sediments) overlying barrier sands (marine sediments) of variable thickness (between 7 and 20 m) and is bounded by a freshwater–brackish water interface towards the continental plain and a freshwater–saltwater interface towards the sea. The underlying aquitard is composed of clay and sandy clay with a variable thickness (between 2 and 20 m). In Punta Médanos, a semi-confined aquifer composed of sand and silty–clayey sand underlying the aquitard/aquiclude can be recognized. In turn, the entire unit overlies a clay layer (Consejo Federal de Inversiones 1989).

The climate of this coastal region is humid temperate and marked by a dry season which coincides—in the southern hemisphere—with the coldest months (April–September) and a rainy season during the warmest months (October–March). The mean annual precipitation fluctuates between 900 and 1000 mm, with 60% occurring in the months with higher evapotranspiration (Carretero and Kruse 2012). Hence, the majority of the recharge occurs during the dry season. Average annual recharge has been estimated to be 230 mm/y (Carretero 2011). Groundwater is recharged on the barrier mainly along the crests of the sand dunes and discharges both to the east towards the sea and to the west towards Samborombon Bay. Tides are mixed, predominantly semidiurnal, with tidal ranges less than 2 m (SHN 2008). In the study area, because of the morphology of the sand-dune barrier, the effects of the tides are limited to the subaerial beach.

The hydrodynamic and hydrochemical behavior of groundwater is determined by the geomorphological environment. In the sand-dune barrier, the water is mainly of the Ca-HCO_3 type (low salinity), whereas in the continental plain, the water is of the Na–Cl type (high salinity) (Carretero et al. 2013b).

Materials and methods

In March 2016, field work was carried out in PDLC to study the SGD. Three methods have been used: hydrogeological measurements in piezometers, ^{222}Rn as a tracer, and electrical tomography. The first two techniques allow for the quantification of groundwater flow, while electrical tomography is a qualitative method and shows the areal distribution of the discharge.

Well studies

Piezometers

A monitoring network constituted by more than 100 piezometers is distributed along the sand-dune barrier from San Clemente to Mar del Tuyú (90 km^2). This sector corresponds to 50% of the PDLC area, but includes more than 60% of the urbanized sectors. Manual measurements were carried out in the monitoring network in March 2016. The data were entered into a geographic information system (GIS) and groundwater flow maps were made from which SGD was calculated. On the basis of the groundwater flow maps, the average hydraulic gradient was estimated as well as an estimated average effective velocity. Using GIS tools and the aquifer parameters (Sy = 0.10; K = 20 m/d), the volume of groundwater was calculated from the maps. It is necessary to clarify that the 0 m.a.s.l. was considered as a boundary which means that the calculated volume is the amount of water storage on the aquifer above the mean sea level. This decision was made taking into consideration that in coastal areas, water levels should not be depleted below mean sea level as a way of reserves preservation and to avoid salt water intrusion.

Burnett et al. (2006) mentioned the piezometers as one of the methods applied for SGD calculation considering the aquifer hydraulic conductivity as a constant and by use of a one-dimensional form of Darcy's Law:

$$Q = -Kdh/dL, \quad (1)$$

where Q is Darcian flux (groundwater discharge volume per unit area per unit time), K is hydraulic conductivity, and dh/dL is the hydraulic gradient in which h is hydraulic head and L is distance. For the study area, the average K is of 20 m/d.

Water balance

To evaluate the hydrological conditions, a daily water balance (Thornthwaite and Mather 1955) was performed allowed for the calculation of the water surplus. The data correspond to the daily precipitation from a rain gauge set in San Clemente del Tuyú for the period April 2015–March 2016. The daily mean reference evapotranspiration (Et_o) data were determined according to the FAO Penman–Monteith method (Allen et al. 1998). The water balance was calculated using the AGROAGUA v.5.0 software (Forte Lay et al. 1995). This software makes it possible to carry out daily water budgets and continuously monitor the soil-water storage, using the daily rainfall, daily potential evapotranspiration, and soil field capacity variables. In the case of immature, sandy soils with sparse vegetation and an effective depth for the water budget of 0.25 m—which characterize the coastal sand-dune barrier—a field capacity of 40 mm was assigned.

Due to the characteristics of the soil (high permeability of the sediments), no surface runoff processes can be observed, and it is considered that the water balance surplus is transformed directly into effective recharge to the aquifer.

Hydrochemistry

Water samples were collected from the sea and from the same wells where Rn was measured. Electrical conductivity (EC) and temperature were measured in situ. The chemical analyses were performed by a private certificated laboratory (GEMA S.R.L) applying the standard methods (Table 1). A Piper Diagram was used for water classification.

Radon measurements

Radon mapping of coastal waters is a technique to locate potential sources of SGD (Stieglitz 2005; Rapaglia et al. 2015). Rn was continuously measured using a Durridge radon-in-air detection system (RAD7) modified to measure radon in water via gas exchange through a Liqui-Cel mini-module membrane filter. A small boat was utilized to travel parallel to the coastline at an average of 3 Kn. The boat attempted to maintain a distance of less than 500 m to the coast wherever possible. Water was pumped into the mini-module via peristaltic pump at a rate of 0.5–0.8 L/min, and the effluent was released back into the sea. Rn activity was continuously measured in the RAD7 as described by Burnett and Dulaiova (2003). Coincident measurements of water temperature and water salinity were collected via a YSI EC 85 conductivity meter. At three separate occasions, the closed system popped open due to back pressure associated with the high suspended sediment concentration from the discharge of the Rio de la Plata. At each occurrence, the boat was stopped until equilibrium was reached. Unfortunately, no samples were collected for suspended sediment concentration, but there was a visual north/south gradient in turbidity, with turbidity decreasing with distance from the river mouth. Wind speed was very low (~ 1–3 m/s) and air temperature fluctuated between 15 °C in the early morning to 28 °C in the early afternoon. Radon activity was later corrected for degassing due to wind as well as for water temperature.

Radon activity was also measured in several wells along the PDLC via the RAD7 technique. Well water was pumped through the mini module until an equilibrium concentration was reached in the detector (~ 35 min). Well samples were collected from wells that were known to be high-quality freshwater wells as well as those that were contaminated with seawater. The well samples were separated into different areas to better constrain the Rn endmember.

Table 1 Methods applied for the chemical analysis

Determination	Method	Detection limit
pH	SM 4500-H + B	0.1 pH units
Calcium	EPA 7140-EAA	0.1 mg/L
Magnesium	EPA 7450- EAA	1 mg/L
Sodium	EPA 7770-EAA	0.02 mg/L
Potassium	EPA 7610-EAA	0.1 mg/L
Iron	EPA 7380-EAA	0.01 mg/L
Manganese	EPA 7460-EAA	0.05 mg/L
Chloride	SM 4500 Cl-B	0.4 mg/L
Sulfate	SM 4500-E	0.5 mg/L
Bicarbonate	SM 2320 B	1 mg/L
Nitrate	SM 4500 NO3 E	0.01 mg/L
TDS	SM 2540 C	1 mg/L
EC	SM 2510-B	1 µS/cm
Bromide	SM 4500 Br-B	0.1 mg/L
Iodide	SM 4500 I-B	0.1 mg/L

Geophysical measurements

The ERT is a method to map the subsurface resistivity distribution in 2D. During the survey, apparent resistivity is measured combining different electrode separation and lateral shifts of the array. The most common arrays are Wenner, dipole–dipole, pole–dipole, and Wenner–Schlumberger arrays (Loke 2015); each one depends on many factors, such as horizontal/vertical sensitivity, signal-to-noise ratio, and strength of the electric field. Resistivity variations can be caused by changes in the lithology, grain size, and even chemical characteristics of groundwater. The large electrical conductivity contrast between seawater (50 µS/cm) and freshwater (1000 µS/cm) makes it possible to map the subsurface groundwater salinity distribution using ERT.

Data acquisition

The survey was conducted along a 35-km line parallel the coast of Buenos Aires in March 2016. A DC resistivity meter and a streamer were set in a boat, and it was positioned with a GPS. The streamer had seven stainless steel electrodes separated at 5 m intervals and it was pulled in contact with the seafloor. A pole–dipole array was used, with three simultaneous measurements and more than 11,600 apparent resistivity data points were acquired in 2 days. The seafloor depths and seawater electrical conductivity were not continuously recorded, but they were manually logged together with their GPS positions.

Data processing

The ERT inversion procedure provides an electrical 2D resistivity distribution that, using a forward model, reproduces the measured data to a specified misfit. The data were processed with RES2DInv using an iterative method of least-squares inversion with smoothness constraints (deGroot-Hedlin and Constable 1990; Sasaki 1992). A seawater layer was considered above the measurement

electrodes, using the seafloor depths and an average value of the measured seawater electrical conductivity (37,000 µS/cm).

Results

Well studies

Water balance

A majority of the annual precipitation (73%) fell during the cold season (Table 2), which is atypical of the normal pattern. Indeed, even though this was an atypical pattern, most of the recharge often occurs during the dry–cold season, as the lowest values of evapotranspiration occur during this season. In other words, evapotranspiration is the most important factor determining recharge. Most of the rain fell during several large events in August 2015. While there was an excessive amount of recharge in the cold season, recharge over evapotranspiration in the warm season was only 7 mm or about 2% of the annual recharge, representing the driest warm season since 2003. The water balance shows that the hydrological conditions during this study were not the average conditions. Recharge during the cold season was very high, while during the previous months to the fieldwork, it was almost null. Meanwhile, March is usually the month with the lowest water levels of the year.

Groundwater flow maps

The maps reflect the hydrological characteristics of the region. The water-table contour maps show that the isophreatic curves increase from north to south. Two main directions of regional discharge can be observed, towards the west to the continental plain and, towards the east, to the sea. The present study focuses in the later (Fig. 2).

In San Clemente, the curves fluctuate between 0.5 and 2 m a.s.l. with the highest water-table heights in the southern sector of the town. The average hydraulic gradient calculated from the maps is about 0.0014.

Las Toninas is characterized by water levels between 1.5 and 3 m a.s.l. with an average hydraulic gradient of 0.0022. Santa Teresita shows the lower water levels; indeed, there are sections along the Coastal Avenue with values below mean sea level and where salt water intrusion was detected. In this town, the highest water level is represented by the 1.5 m a.s.l. curves and the hydraulic gradient is of 0.0019.

In Mar del Tuyú, the curves vary from 1.5 to 4 m a.s.l. being the town with the highest water-table heights and a hydraulic gradient of 0.0033.

Hydrochemistry

Most of the groundwater samples located in the sand-dune barrier are marked by low EC (< 1500 µS/cm) and are classified as Ca-HCO_3 (Table 3). The exceptions are wells SC-H, ND9, and ST4 which are NaCl type and CaNa type, respectively, but, here, the EC values are between 900 and 2000 µS/cm. Sample SC1 and ST12 are also NaCl type but with very

Table 2 Results of the water balance for a hydrological year and the cold and warm season

		Month	P[a] (mm)	PET[b] (mm)	AET[c] (mm)	Surplus (mm)
Hydrological year	Cold season	Apr-15	34	67.8	24.1	0
		May-15	140	49	37.4	88.7
		Jun-15	0	37.1	18.3	0
		Jul-15	70	37.2	11.3	29.7
		Aug-15	236	48.9	42.6	205.2
		Sep-15	15	58.2	26.5	0
		Total	495	298	160	324
	Warm season	Oct-15	42	65.1	42.8	0
		Nov-15	24	63	24.6	0
		Dec-15	45	63	26.2	7
		Jan-16	0	65.5	19.9	0
		Feb-16	37	64.3	25.7	0
		Mar-16	38	75.3	40.9	0
		Total	186	396	180	7
		Total year	681	694	340	331

[a] *P* precipitation

[b] *PET* potential evapotranspiration

[c] *AET* actual evapotranspiration

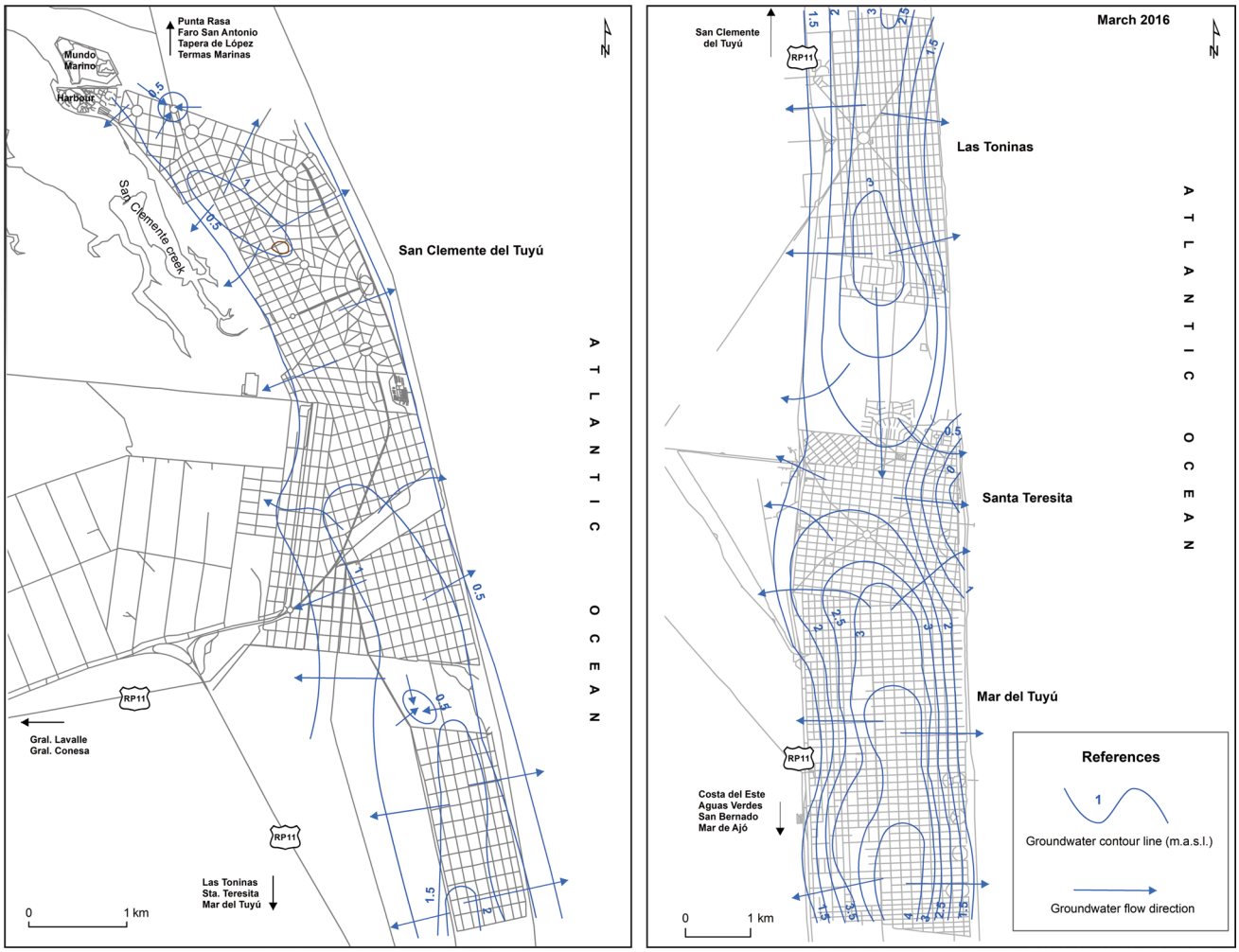

Fig. 2 Groundwater flow maps for March 2016. Left, San Clemente del Tuyú; right, sector including Las Toninas, Sta. Teresita and Mar del Tuyú

high EC. The first is due to the well which is located in the transition to the continental plain and the second is affected by saltwater intrusion.

Seawater samples present values of EC from 27,600 to 43,200 µS/cm rising from north (Punta Rasa) to south (Costa del Este). Sample Sea0 was taken in the limit of the Río de la Plata estuary and the Atlantic Ocean (Argentine Sea), so the influence of the estuary is reflected in the salinity and lower concentration of anions and cations in comparison with samples Sea1 and Sea2 (Table 3).

The presence of high concentrations of Fe and Mn in groundwater, which is a source of drinking water supply to the population, is a relatively common problem in several coastal regions; the PDLC can be included among them (Carretero and Kruse 2015). The values above the admissible levels for human consumption extend over an area that includes most of the aquifer located in the coastal dunes.

Fe concentrations in groundwater samples for this work are below < 0.01 mg/L which is the detection limit of the instrument except for in well ST12 which concentration is 13.2 mg/L. Mn shows values between < 0.05 (detection limit) and 0.7 mg/L with a mean value of 0.56 mg/L. Meanwhile, in the coastal Atlantic Ocean, both Fe and Mn concentrations are below the detection limits.

During previous sampling campaigns (2013–2016) for the same wells, Fe concentrations fluctuate between < 0.01 and 0.44 mg/L, with a mean value of 0.24 mg/L. Mn varies between < 0.05 and 1.20 mg/L, with a mean value of 0.58 mg/L.

A survey of domestic wells was undertaken in 2006 (Carretero and Kruse 2015) which showed that Fe concentrations in groundwater vary from 0.03 to 3.5 mg/L, with a mean value of 0.33 mg/L, while Mn varies between 0.03 and 1.20 mg/L, with a mean value of 0.24 mg/L.

Table 3 Radon activity and chemical composition for groundwater and seawater

	Groundwater									Seawater		
	SC1	SC14	SC17	SC25	SC–H	ND9	ST11	ST4	ST12	[1]SEA0	[2]SEA1	[3]SEA2
EC (μS/cm)	18772	1122	818	805	913	1762	787	2033	30600	27600	42200	43200
TDS (mg/L)	9520	570	374	386	464	880	379	1031	16600	13800	21100	21600
pH	7.95	8.13	8.22	8.15	7.95	7.83	7.95	7.78	7.86	7.62	7.23	7.55
Ca (mg/L)	1521	120.7	185	51.2	50.4	221	72.3	662	4704	556	862.3	864.3
Mg (mg/L)	1210	17.9	14.5	33.4	27.2	11.0	8.9	9.9	1056	1572	2061.6	2489
Na (mg/L)	8650	165	68	97	198	496	172	226	18750	13690	21680	17650
K (mg/L)	302.3	18.7	10.7	17.2	21.9	17.8	10.6	7.4	209	493	635.3	799
Fe (mg/L)	< 0.01	< 0.01	< 0.01	< 0.01	< 0.01	< 0.01	< 0.01	< 0.01	13.2	< 0.01	< 0.01	< 0.01
Mn (mg/L)	0.60	< 0.05	< 0.05	< 0.05	< 0.05	< 0.05	< 0.05	0.38	0.70	< 0.05	< 0.05	< 0.05
Cl (mg/L)	16301	201	124.4	125.8	278.4	848	122.3	591	30269	23141	42240	38331
SO_4 (mg/L)	825	38.4	14.5	31.3	17.1	23.3	3.6	44.4	530	350	2030	350
HCO_2 (mg/L)	390	490	320	330	300	500	490	620	180	125	160	140
NO_3 (mg/L)	92.5	2.0	0.7	1.9	1.3	1.8	0.40	2.8	144	173	196	362
NO_2 (mg/L)	< 0.01	< 0.01	< 0.01	< 0.01	< 0.01	< 0.01	< 0.01	< 0.01	< 0.01	ND	ND	ND
Br (mg/L)	ND	ND	ND	ND	ND	ND	ND	ND	ND	0.10	0.10	0.10
I (mg/L)	ND	ND	ND	ND	ND	ND	ND	ND	ND	< 0.1	< 0.1	0.15
Water type	NaCl	Ca-HCO_3	Ca-HCO_3	Ca-HCO_3	NaCl	NaCl	Ca-HCO_3	CaCl	NaCl	NaCl	NaCl	NaCl
^{222}Rn (dpm/L)	105.6 ± 17.3	81.6 ± 11.5	15.65 ± 5.6	172.8 ± 17.3	44.45 ± 8.6	110.4 ± 13.4	148.22 ± 15.6	146.5 ± 15.6	127.2 ± 14.4	19.78 ± 6	6.12 ± 3.64	1.35 ± 2.19

Seawater samples taken in the area of [1]Punta Rasa, [2]Las Toninas, [3]Costa del Este

ND not determined

Fe and Mn are found in high concentrations in other coastal barrier environments such as the southern Brazil barrier spit separating the Patos Lagoon, the largest coastal lagoon in South America, from the South Atlantic Ocean (Windom et al. 2007). In this area, permanent wells and beach wells were analyzed showing Fe concentrations between 0.74 and 1.63 mg/L and Mn values from 0.11 to 0.24 mg/L. These authors also mentioned concentrations for the ocean taken from Bruland (1983) being 0.0001 and 0.00003 mg/L for Fe and Mn, respectively. In the same study area, Windom et al. (2006) reported that Fe and Mn concentrations ranged from 0.035 to 10.53 mg/L and from 0.003 to 0.93 mg/L, respectively. These values are in the range of the values reported for the freshwater region of the subterranean estuary in the Waquoit Bay, USA (Charette and Sholkovitz 2006) where Fe concentrations vary from 2.93 to 10.24 mg/L and Mn concentrations fluctuate between 0.82 and 2.2 mg/L.

On the barrier islands constituting North Carolina's Outer Banks, freshwater occurs in small, isolated, lens-shaped masses above denser saltwater in the surficial aquifer (Winner 1975; Winner and Coble 1996). Freshwater on the Outer Banks is of general good quality with a few problems associated with local conditions as the case of Fe concentrations reaching a maximum of 2 mg/L.

Fe, Mn, and NO_3 were measured at seven wells during periods of low and high groundwater flow, in the aquifer around Flanders Bay in Eastern Long Island, New York (Montluçon and Sañudo–Wilhelmy 2001). For the first scenario, Mn concentrations range from 0.01 to 5 mg/L, Fe values fluctuates between 0.07 and 25.9 mg/L, and NO_3 presents a predominant distribution between 0.04 and 10.4 mg/L. For the second scenario, Mn, Fe, and NO_3 concentrations vary from 0.02 to 0.73 mg/L, 0.01 to 10.71 mg/L, and 0.001 to 50.8 mg/L, respectively.

It is well known that high concentrations of nitrates in drinking water lead to health problems. For the samples taken in March 2016, in PDLC area, NO_3 concentrations in groundwater fluctuate from 1.3 to 2.9 mg/L with high concentrations in wells SC1 and SC12 (92 and 144 mg/L) associated with the coastal plain environment and the saltwater intrusion phenomenon. Seawater samples present values from 173 to 362 mg/L.

In the above-mentioned investigation (Carretero and Kruse 2015), NO_3 values vary between 9 and 21 mg/L with two samples in the semi-urbanized area presenting concentrations higher than 50 mg/L (97 and 180 mg/L). Nitrites show values between 0.01 and 0.03, with 50% appearing below the detection limit of 0.01 mg/L. In 2016, NO_2 concentrations show values below the detection limit. The specific cases with elevated values are attributed to anthropogenic contamination due to the proximity to septic tanks.

In Great South Bay (Long Island, USA) coastal environment, Capone and Bautista (1985), Monti and Scorca (2003), and the New York State, Department of Environmental Conservation Report (2014) investigated NO_3 concentrations in the groundwater of the barrier island. Median groundwater NO_3 levels in the Upper Glacial Aquifer were of 15.85 mg/L. The median NO_3 concentration in Nassau County (during 1952–1997) was 0.66 mg/L with values ranging from <0.044 to 55.84 mg/L. For Suffolk County, median was <0.44 mg/L and values ranged from <0.044 to 21.83 mg/L. Higher NO_3 concentrations in this area (84.13 mg/L) were previously found by Smith and Myott (1975). A summary of these data can be seen in Table 4.

Radon measurements

Radon activity generally decreased with distance from the mouth of the Rio de la Plata (highest in the northern end of the study area–lowest in the southern end of the study area) (Fig. 3). Although no suspended sediment samples were taken, there existed a strong visual gradient in turbidity with distance from the mouth, this gradient seemed to correlate with radon activity. The Rio de la Plata turbidity front is a well-known phenomenon (Framiñan and Brown 1996) and activity significantly decreased as we moved outside the turbidity zone. Overall, radon activity decreased from 20.5 ± 7.2 to 1.3 ± 3.4 dpm/L as we moved southward along the coast. There were smaller fluctuations in radon activity found at Km12 and Km20 of our study transect.

Radon activity in wells was fairly stable around the PDLC. In many SGD studies, a large source of uncertainty is due to high variability in endmember activity (e.g., Povinec et al. 2008; Cerdà-Domènech et al. 2017; Cho and Guebuem 2016), but, in this case, there was little variability only fluctuating by circa 40% and had values averaging 130 ± 45 dpm/L, with the exception of SC17 well which had a low activity, and was very difficult to pump (here, Rn values were only $\sim 15 \pm 6$ dpm/L). Rn activity in tidal pools ($\sim 50 \pm 12$ dpm/L) and in the surf zone ($\sim 30 \pm 14$ dpm/L) was relatively high when compared to that found in our coastal transect. Rn activity in air was negligible (~ 0.3 dpm/L). A Radon diffusion experiment was run by placing allowing sediment in 30 L of fresh water to diffuse over a 40 min period. Diffusion reached equilibrium at 8 dpm/L.

It is difficult to quantify SGD via Rn activity along an open coastline as mixing of waters is hard to characterize, and the so-called flux-in component of the mass balance is not as clear as it would be in a coastal lagoon (Stieglitz et al. 2010). However, if we make the assumption that Rn input from the open ocean is negligible, we can create a mass balance to help quantify SGD along the coastline.

Table 4 Fe, Mn, and NO_3 concentrations in groundwater in coastal barrier environments

Authors	Site	Fe (mg/L)	Mn (mg/L)	NO_3 (mg/L)
This work (March 2016)	PDLC	< 0.01–13.2	< 0.05–0.7	1.3–2.9
Carretero unpublished data (2013–2016)	PDLC	< 0.01–0.44	< 0.05–1.2	
Carretero and Kruse (2015)	PDLC	0.03–3.5	0.03–1.2	9–21
Windom et al. (2007)	Southern Brazil barrier spit, Los Patos Lagoon area	0.74–1.63	0.11–0.24	
Windom et al. (2006)	Southern Brazil barrier spit, Los Patos Lagoon area	0.035–10.53	0.003–0.93	
Charette and Sholkovitz (2006)	Waquoit Bay, USA	2.93–10.24	0.82–2.2	
(Winner 1975; Winner and Coble 1996)	North Carolina's Outer Banks	Maximum 2		
Montluçon and Sañudo–Wilhelmy (2001)	Flanders Bay in Eastern Long Island, New York, USA	0.07–25.9/0.01–10.71	0.01–5/0.02–0.73	0.04–10.4/0.001–50.8
Capone and Bautista (1985); Monti and Scorca (2003); New York State, Department of Environmental Conservation Report (2014)	Great South Bay, Nassau County. (Long Island, USA)			< 0.044–55.84
	Great South Bay, Suffolk County. (Long Island, USA)			< 0.044–21.83

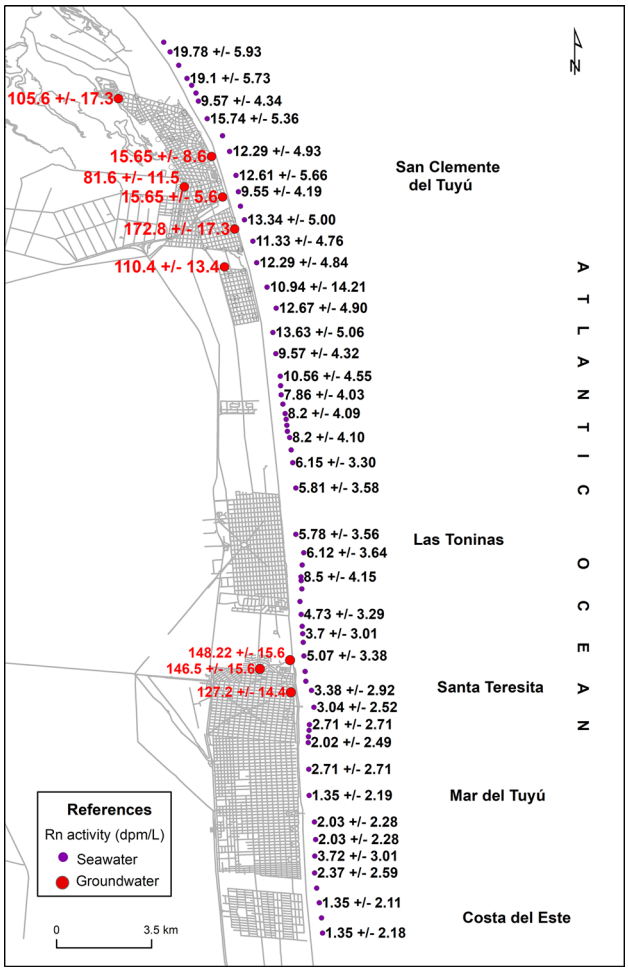

Fig. 3 Radon activity in seawater and groundwater

The sources and the sinks of ^{222}Rn in coastal waters can be described in a mass balance model as (Burnett and Dulaiova 2003)

$$F_{SGD} + F_{Diff} + F_{Riv} = F_{atm} + F_{dec} + F_{mix} \quad (2)$$

with $F_{SGD} = {}^{222}Rn$ flux from SGD (Bq/m^2/d), $F_{diff} = {}^{222}Rn$ flux originating from diffusion from sediments, $F_{Riv} = {}^{222}Rn$ river supply; F_{atm} = loss of ^{222}Rn by atmospheric evasion; F_{dec} = decay of ^{222}Rn in the water column; F_{mix} = loss of ^{222}Rn due to mixing.

In the following, we assume F_{diff} to be of minor importance for the regional differences in the ^{222}Rn distribution which we are discussing here. While there is a significant river entering into this area, we do not yet have the ability to constrain the amount of Rn, which may be entering into this area through the river, so we will assume that it is negligible and hence report the highest possible amount of radon entering through SGD, thereby likely overestimating the role of SGD in the area. Meanwhile, as this is an open coastline, it is difficult to attempt constraining the mixing to the open sea from outside the box.

Thus, Eq. 2 simplifies to

$$F_{SGD} = F_{atm} + F_{dec} \quad (3)$$

.

Equation 3 shows the loss of ^{222}Rn due to atmospheric evasion (F_{atm}) and $F_{dec,}$ which can be determined by measuring the ^{222}Rn inventory, i.e., the seawater ^{222}Rn concentration times the water depth multiplied by the ^{222}Rn decay constant.

Atmospheric evasion is calculated by multiplying the gas transfer coefficient for Rn by the average radon concentration

in the open water. The portioning coefficient is neglected as it is multiplied by the negligible amount of Rn in open air. The gas transfer coefficient is based on wind speed, with the greater the wind speed, the greater the atmospheric evasion. Wind speed was quite low during our study period; hence, atmospheric evasion should also be relatively negligible. Therefore, the major factor determining the mass balance is decay, which is dependent upon the depth of the water and the surface Rn concentration.

The radon flux due to SGD can then be divided by the average SGD activity in the wells to determine the SGD flux in $m^3/m/d$. This flux will be divided into separate sections along the coastline.

Geophysical measurements

The ERT resistivity sections (Fig. 4) showed a top layer of with resistivity ranges of 0.25–0.5 Ohm m with a thickness of 1 m. The next layer between 3 and 4 m beneath the seafloor appears to show increasing resistivity values of about 1–5 Ohm m. This increment may indicate a mixing zone of freshwater and saltwater in the sandy aquifer layer. The lowest resistivity values present in the inverted resistivity section are interpreted as the presence of saltwater. Resistivity values over 5 Ohm m were observed at 3520, 9920, 15,040, and 24,000 m of the transect, which can be because of increasing thickness of freshwater of the mixing zone.

Calculation of potential SGD via different methods

Hydrological measurements

Submarine groundwater discharge values calculated from the water-table flow maps expressed in m^3/d per meter of coastline ($m^3/m/d$) are 0.21, 0.41, 0.38, and 0.57 for San Clemente, Las Toninas, Santa Teresita, and Mar del Tuyú, respectively. The average SGD for the entire area would be of 0.39 $m^3/m/d$.

The amount of groundwater above mean sea level, in March 2016, calculated from the maps is 1,693,401 m^3 (1.69 hm^3) for San Clemente and of 9,478,735 m^3 (9.48 hm^3) for the sector including Las Toninas, Sta. Teresita, and Mar del Tuyú. The total volume is about 11,172,136 m^3 (11.17 hm^3). Discharge for the total length of coastline in the first sector is 1549 m^3/d and for the second 6557 m^3/d. Total discharge is 8106 m^3/d which represents 0.07% of the groundwater volume.

Rn measurements

Using our corrected Rn data, we can develop a potential mass balance for the northern 27 km of the coast of the PDTLC. If we assume that Rn is in equilibrium, then our sources must equal our sinks. Here, the sinks of Rn include atmospheric evasion, decay, and mixing out of our box. The

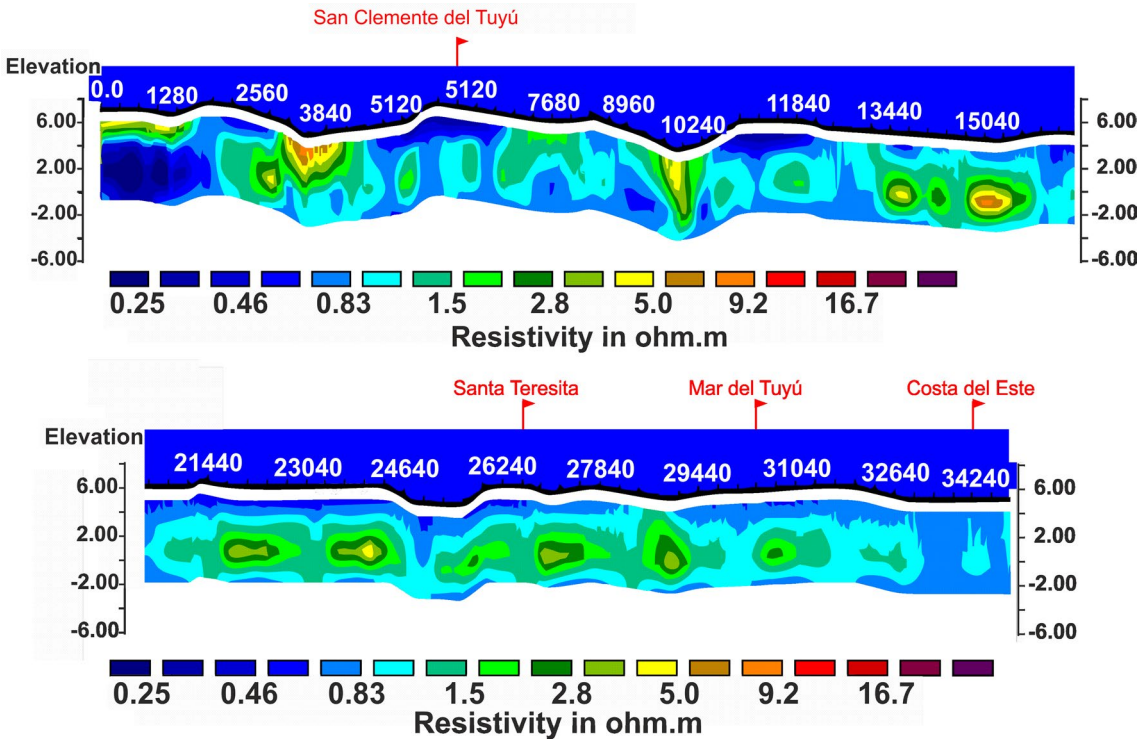

Fig. 4 ERT resistivity sections

sources include mixing into the box, diffusion from sediments, and advection via SGD. If we assume that the mixing into and out of the box is equivalent, we can then narrow our sources down to diffusion from sediments (which we previously assumed negligible) or SGD. Another complication is the lack of data concerning the residence time of the water in our system. Hence, the decay term is marked by uncertainty. Based on an understanding of the hydrodynamic field here, we can estimate that the residence time is on the order of one half life. As there are several layers of uncertainty, we need to perform an analysis of uncertainty propagation following the method described in the National Institute of Standards and Technology (NIST) (Taylor and Kuyatt 1994). We will only propagate uncertainty for the numbers that we know, hence, we cannot take into account uncertainty from riverine flux and mixing with the open ocean. Therefore, this is only a first estimate at best.

We have split the PDTLC into two sections: San Clemente and Santa Teresita. In San Clemente, the average Rn activity was 14.2 ± 6.8 dpm/L and the average well activity was 140 ± 67 dpm/L. In Santa Teresita, the average Rn activity was 4.6 ± 2.7 dpm/L and the average well activity was 202 ± 17 dpm/L. In San Clemente, therefore, the SGD flux is calculated to be 3.2 ± 2.4 m^3/s, and for Santa Teresita, it is 0.4 ± 0.3 m^3/s. Using the average Rn activity in water (7.3 ± 4.2 dpm/L) and average well activity of 138 ± 45 (dpm/L) for the endmember, we can attempt to calculate the total SGD flux. Our values indicate that the total flow of SGD from the Partido de La Costa is 1.1 ± 0.6 m^3/s or 3.5 ± 2.5 m^3/m/d. This is an order of magnitude higher than SGD calculated via Darcy's Law. Potential reasons for this include uncertainty in the residence time, uncertainty in the endmember value, inclusion of recirculated seawater, and complications due to high turbidity in the northern end of the PDLC due to river inputs. Further tests can be done to narrow down the uncertainty in these parameters.

Discussion

There is much concern along the Partido de La Costa, Argentina that their freshwater resources are declining due to overpumping and the intrusion of seawater into the freshwater lens below the barrier. To better understand groundwater–seawater interactions in the PDTLC, it was advantageous to incorporate classical hydrogeology with direct and indirect measurements of submarine groundwater discharge. Both flow based on Darcy's Law and quantification of SGD via Radon suggest that the overall movement of water across the sediment–sea interface is from the aquifer to the sea, meaning that there is a net positive outflow along the studied area.

The outflow of water from the coastal aquifer to the sea, however, does not seem to be consistent throughout the study area, but rather highly spatially variable, with areas of relatively large SGD interspersed with areas of salt water intrusion. Both hydrogeological parameters and electrical resistivity measurements find pockets of high groundwater salinity near villages, which are pumping water directly, instead of from the controlled well field. We hoped that the Radon signal would also pick up this pattern, with areas of relatively low surface water radon concentration found near sites of saltwater intrusion. If this was the case, it would provide support for the hypothesis that Rn could be used as a relatively quick mapping method for SGD. However, due to mixing of surface waters, the spatial signal is likely diluted by the time which waters are circa 300 m offshore from the beach. Resistivity measurements, however, seem to have more potential to locate salt water intrusion. Meanwhile, no spatial trend in Rn activity along the PDLC was seen, nor was there a correlation between Rn activity and groundwater salinity or the other chemical parameters analyzed.

Due to potential temporal variability in groundwater flow as well as measurement error and endmember uncertainty, SGD as quantified by Radon vs. Darcy's Law differed by an order of magnitude, which is most likely due to the unknown input of Rn due to input via the river. This difference suggests that, although beneficial to have a multi-parameter study, it is likely important to repeat the process over several time periods to better delineate the temporal variability in radon SGD quantification. It is also particularly hard to estimate the exchange of Rn to the open sea, in an unenclosed embayment. Hence, Rn may be better served in these environments to confirm the presence and location of SGD, rather than to quantify it.

Potentially more interesting than the SGD quantification is the utility of these techniques to map where groundwater may be flowing. Both the geophysical measurements and the Rn activity can be used to map where groundwater may be flowing in real time. Meanwhile, the extensive hydrological data can be used to show if these patterns exist in a well field to well-field basis.

Conclusion

In the study area, SGD has been detected via three complementary approaches. The hydrodynamics and the use of radon allowed making a quantification, while the geophysical method was qualitative and shows the spatial distribution of the SGD along the coastline. These results represent the hydrological situation for March 2016. This is a highly dynamic system; for this reason, it is not recommended to extrapolate these values to other months and make annual calculation of the SGD.

The 2D models obtained from the ETR allowed identifying a zone below the seafloor with a resistivity higher than the sea water resistivity that might be assumed to a freshwater–saltwater mixing zone caused by the SGD. This zone was detected along the profile between 3 and 4 m depth below seafloor.

The quantification has given SGD values of 0.39 m^3/m/d according to Darcy's Law and of 3.5 (± 2.5) m^3/m/d using radon which is one order of magnitude higher. Further tests can be done to narrow down the uncertainty in these parameters.

There are no previous studies in the area applying the combination of these methods. In fact, this is the first approach using radon as a tracer along Buenos Aires coast. This is an important contribution for the coastal hydrodynamic investigation in the region.

Acknowledgements The authors would like to thank the Cooperativa de Provisión de Obras y Servicios Públicos de San Clemente del Tuyú Ltda. for their collaboration. This work was supported by the Consejo Nacional de Investigaciones Científicas y Técnicas of Argentina, grant number PIP 0403, 2013–2015, and the Agencia Nacional de Promoción Científica y Tecnológica, grant number PICT 2013-2117, 2014–2017.

References

Allen RG, Pereira LS, Raes D, Martin Smith M (1998) Crop evapotranspiration. Guidelines for computing crop water requirements, FAO irrigation and drainage papers 56. FAO, Rome

Barlow PM, Reichard EG (2010) Saltwater intrusion in coastal regions of North America. Hydrogeol J 18(1):247–260

Bruland KW (1983) Trace elements in seawater. Chemical oceanography, vol 8. Academic Press, London, pp 157–220

Burnett WC, Dulaiova H (2003) Estimating the dynamics of groundwater input into the coastal zone via continuous radon-222 measurements. J Environ Radioact 69(1–2):21–35

Burnett WC, Aggarwal PK, Aureli A, Bokuniewicz H, Cable JE, Charette MA, Kontar E, Krupa S, Kulkarni KM, Loveless A, Moore WS, Oberdorfer JA, Oliveira J, Ozyurt N, Povinec P, Privitera AMG, Rajar R, Ramessur RT, Scholten J, Stieglitz T, Taniguchi M, Turner JV (2006) Quantifying submarine groundwater discharge in the coastal zone via multiple methods. Sci Total Environ 367(2–3):498–543

Cable JE, Burnett WC, Chanton JP, Weatherly GL (1996) Estimating groundwater discharge into the northeastern Gulf of Mexico using radon-222. Earth Planet Sci Lett 144(3–4):591–604

Capone DG, Bautista MF (1985) A groundwater source of nitrate in nearshore marine sediments. Nature 313(5999):214

Carretero S (2011) Comportamiento hidrológico de las dunas costeras en el sector nororiental de la provincia de Buenos Aires [Hydrological behavior of coastal dunes on the northeastern coast of Buenos Aires province]. PhD thesis. Facultad de Ciencias Naturales y Museo, Universidad Nacional de La Plata, La Plata. Argentina. http://sedici.unlp.edu.ar/search/request.php?id_document=ARG-UNLP-TPG-0000002075&request=request. Accessed 10 Mar 2018

Carretero S, Kruse E (2010) Areal exploitation of groundwater in coastal dunes, Buenos Aires, Argentina. In: Paliwal BS (ed) Global groundwater resources and management. Scientific Publishers, India, Jodhpur, pp 385–398

Carretero S, Kruse E (2012) Relationship between precipitation and water-table fluctuation in a coastal dune aquifer: northeastern coast of the Buenos Aires province, Argentina. Hydrogeol J 20:1613–1621

Carretero S, Kruse E (2015) Iron and manganese content in groundwater on the northeastern coast of the Buenos Aires Province, Argentina. Environ Earth Sci 73(5):1983–1995

Carretero S, Dapeña C, Kruse E (2013a) Hydrogeochemical and isotopic characterisation of groundwater in a sand-dune phreatic aquifer on the northeastern coast of the province of Buenos Aires. Isot Environ Health Stud 49(3):399–419

Carretero S, Rapaglia J, Bokuniewicz H, Kruse E (2013b) Impact of sea level rise on saltwater intrusion length into the coastal aquifer, Partido de La Costa, Argentina. Cont Shelf Res 61–62:62–70

Cerdà-Domènech M, Rodellas V, Folch A, Garcia-Orellana J (2017) Constraining the temporal variations of Ra isotopes and Rn in the groundwater end-member: implications for derived SGD estimates. Sci Total Environ 595:849–857

Charette MA, Sholkovitz ER (2006) Trace element cycling in a subterranean estuary: Part 2. Geochemistry of the pore water. Geochimica et Cosmochimica Acta 70(4):811–826

Cho HM, Guebuem K (2016) Determining groundwater Ra end-member values for the estimation of the magnitude of submarine groundwater discharge using Ra isotope tracers. Geophys Res Lett 43(8):3865–3871

Consejo Federal de Inversiones (1989) Evaluación del Recurso Hídrico Subterráneo de la Región Costera Atlántica de la Provincia de Buenos Aires. Regiones 1 y 2. Punta Rasa-Punta Médanos. Provincia de Buenos Aires. Informe Final, Geología y Geomorfología [Evaluation of groundwater resources in the Atlantic Coastal Region of Buenos Aires province. Regions 1 and 2. Punta Rasa-Punta Médanos. Buenos Aires province. Final Report, Geology and Geomorphology]. Consejo Federal de Inversiones, Buenos Aires

deGroot-Hedlin C, Constable S (1990) Occam's inversion to generate smooth, two dimensional models form magnetotelluric data. Geophysics 55:1613–1624

Forte Lay JA, Aiello JL, Kuba J (1995) Software AGROAGUA v.5.0. AGROAGUA, CIBIOM. CONICET. Buenos Aires

Framiñan MB, Brown OB (1996) Study of the Río de la Plata turbidity front, Part 1: spatial and temporal distribution. Cont Shelf Res 16(10):1259–1282

Johannes RE (1980) The ecological significance of the submarine discharge of groundwater. Mar Ecol Prog Ser 3:365–373

Loke MH (2015) Tutorial: 2-D and 3-D electrical imaging surveys. Geotomo Software, Malaysia

Monti J Jr, Scorca MP (2003) Trends in nitrogen concentration and nitrogen loads entering the South Shore Estuary Reserve from streams and ground-water discharge in Nassau and Suffolk counties, Long Island, New York. US Geological Survey, New York, pp 1952–1997 **(No. 2002-4255)**

Montluçon D, Sañudo-Wilhelmy SA (2001) Influence of net groundwater discharge on the chemical composition of a coastal environment: flanders Bay, Long Island, New York. Environ Sci Technol 35(3):480–486

Mulligan A, Charette MA (2006) Intercomparison of submarine groundwater discharges estimates from an unconfined sandy coastal aquifer. J Hydrol 327:411–425

New York State, Department of Environmental Conservation Report (2014) Suffolk County: addressing the consequences of development without adequate sewer and septic systems. https://www.dec.ny.gov/lands/97030.html. Accessed 16 Jun 2019

Paytan A, Shellenbarger GG, Street JH, Gonneea ME, Davis K, Young MB, Moore WS (2006) Submarine groundwater discharge: an important source of new inorganic nitrogen to coral reef ecosystems. Limnol Oceanogr 51(1):343–348

Povinec PP, Bokuniewicz H, Burnett WC, Cable J, Charette M, Comanducci JF, Kontar E et al (2008) Isotope tracing of submarine groundwater discharge offshore Ubatuba, Brazil: results of the IAEA-UNESCO SGD project. J Environ Radioact 99(10):1596–1610. https://doi.org/10.1016/j.jenvrad.2008.06.010

Rapaglia J, Grant C, Bokuniewicz H, Pick T, Scholten J (2015) A GIS typology to locate sites of submarine groundwater discharge. J Environ Radioact 145:10–18

Sasaki Y (1992) Resolution of resistivity tomography inferred from numerical simulation. Geophys Prospect 40:453–464

Sherif MM, Singh VP (1999) Effect of climate change on sea water intrusion in coastal aquifers. Hydrol Process 13(8):1277–1287

SHN (2008) (Servicio de Hidrografía Naval) [Naval Hydrographic Service] Tabla de Mareas [Tide Table]. In: Pub. H-610, Armada Argentina, Buenos Aires

Slomp CP, Van Cappellen P (2004) Nutrient inputs to the coastal ocean through submarine groundwater discharge: controls and potential impact. J Hydrol 295(1–4):64–86

Smith SO, Myott DH (1975) Effect of cesspool discharge on groundwater quality on Long Island, NY. J Am Water Works Assoc 67(8):456–458

Stieglitz T (2005) Submarine groundwater discharge into the nearshore zone of the Great Barrier Reef, Australia. Mar Pollut Bull 51(1–4):51–59

Stieglitz T, Rapaglia J, Bokuniewicz H (2008) Estimation of submarine groundwater discharge from bulk ground electrical conductivity measurements. J Geophys Res Oceans 113:C8

Stieglitz TC, Cook PG, Burnett WC (2010) Inferring coastal processes from regional-scale mapping of 222 radon and salinity: examples from the Great Barrier Reef, Australia. J Environ Radioact 101(7):544–552

Taylor BN, Kuyatt CE (1994) NIST technical note 1297. Guidelines for evaluating and expressing the uncertainty of NIST measurement results, 24

Thornthwaite C, Mather J (1955) The water balance Climatol 8:1–37

Werner AD, Simmons CT (2009) Impact of sea-level rise on sea water intrusion in coastal aquifers. Groundwater 47(2):197–204

Windom HL, Moore WS, Niencheski LF, Jahnke RA (2006) Submarine groundwater discharge: a large, previously unrecognized source of dissolved iron to the South Atlantic Ocean. Mar Chem 102:252–266

Windom H, Moore W, Niencheski F (2007) Influence of groundwater discharge through a coastal sandy barrier in southern Brazil on seawater metal chemistry. A new focus on groundwater–seawater interaction. IAH International Commission on Groundwater. XXI General Assembly, IUGG: 180–188

Winner Jr MD (1975) Ground-water resources of the Cape Hatteras National Seashore, North Carolina: U.S. Geological Survey Hydrologic Investigations Atlas HA-540, 2 sheets

Winner Jr MD, Coble RW (1996) Hydrogeologic framework of the North Carolina coastal plain. Professional Paper 1404- I. https://doi.org/10.3133/pp1404I. Accessed 16 June 2019